Electronic supplementary information

Backbone-Driven Host-Dopant Miscibility Modulates Molecular Doping in NDI Conjugated Polymers

Diego Rosas Villalva, Saumya Singh, Luke A. Galuska, Anirudh Sharma, Jianhua Han, Jian Liu, Md Azimul Haque, Soyeong Jang, Abdul Hamid Emwas, L. Jan Anton Koster, Xiaodan Gu, Bob C. Schroeder,* Derya Baran*

Experimental Section

Synthesis:

Materials

All reagents and anhydrous solvents were purchased from commercial sources (SigmaAldrich, TCI, and VWR) and used as received. NDI monomer 1 was synthesized according to our previous report.[1]

General procedure for the polymer synthesis:

In a 20 mL microwave vial, NDI monomer **1** (400 mg, 0.338 mmol) and 1 eq of the corresponding stannylated monomer (5,5'-bis(trimethylstannyl)-2,2'-bithiophene (166 mg) for P1G and Bis(trimethylstannyl)acetylene (119 mg) for P3G) were dissolved in 15 mL of anhydrous, degassed chlorobenzene. $Pd_2(dba)_3$ (2 mol%) and P(*o*-tol)$_3$ (8 mol%) were added and the reaction mixture was purged with nitrogen for 10 min. The vial was sealed and heated to 125 °C – 130 °C for 20 hours. For end-capping, chlorobenzene solution of 2-Tributylstannyl)thiophene (5 mol%) and $Pd_2(dba)_3$ were added to the vial, and the reaction mixture was heated for 2 hours followed by the addition of 2-bromothiophene (10 mol%), and the reaction was continued for another 2 hours.

After end-capping, the reaction mixture was cooled to room temperature. The crude reaction mixture was then precipitated in cold hexane. The solid obtained was directly filtered into a glass-fiber thimble. Soxhlet extraction was carried out with methanol, acetone, and hexane to remove unreacted monomers and oligomers. Final extraction was done with chloroform to collect polymer. The chloroform fraction was concentrated under reduced pressure and precipitated from cold hexane to obtain a pure polymer.

P1G: After purification, P1G was obtained as a dark blue solid (310 mg, 77 %). GPC (dichlorobenzene, 80 °C): Mn = 21,371 g·mol^{-1}, Mw = 31,530 g·mol^{-1}, and Đ = 1.5

^{1}H NMR (400 MHz, $CDCl_3$) δ: 8.81 (s, 2H), 7.36 (broad, 4H), 4.29 (broad, 4H), 3.61 – 3.50 (m, 56H), 3.35 (broad, 12H), 2.55 (m, 2H).

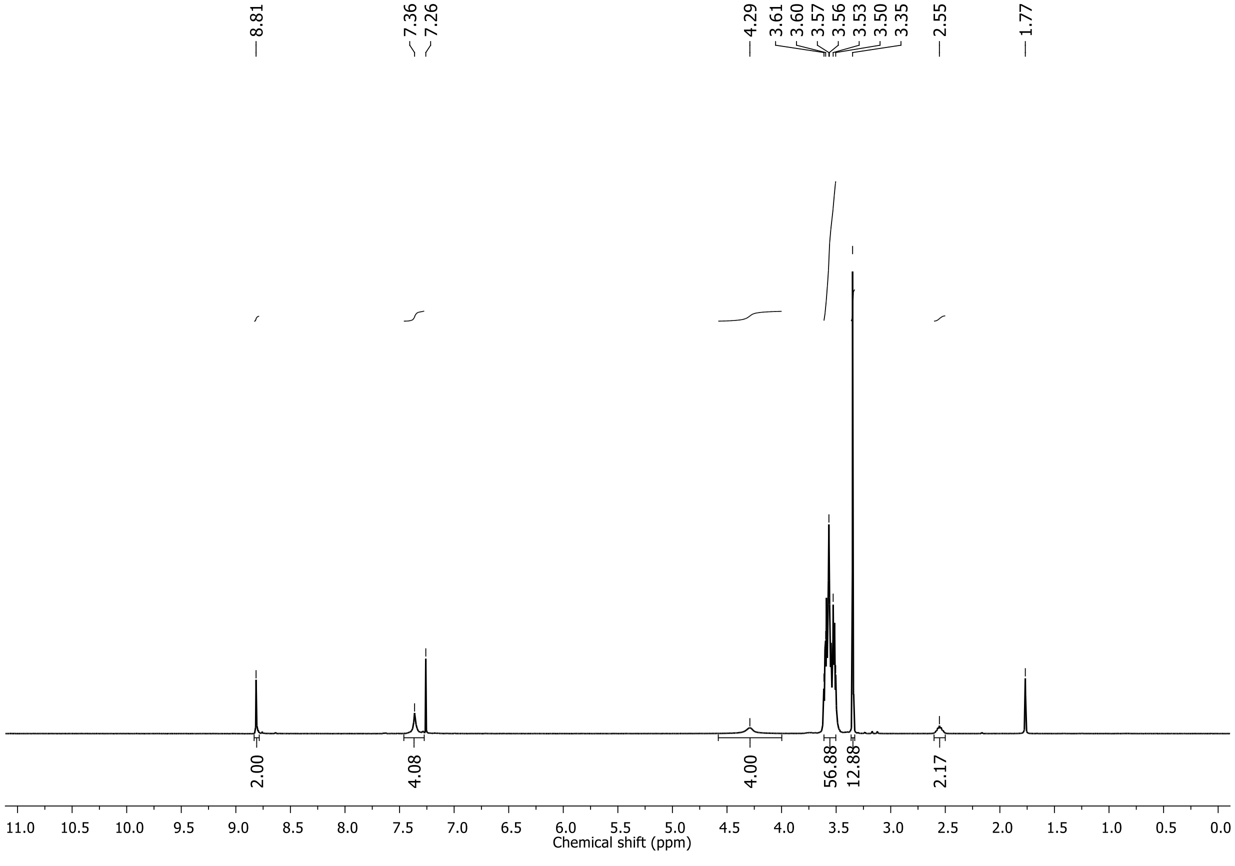

Figure S1: ^{1}H NMR spectrum of polymer P1G in $CDCl_3$.

P3G: After purification, P3G was obtained as a dark red solid (100 mg, 28 %). ^{1}H NMR (400 MHz, TCE-*d*$_2$) δ: 9.13 (s, 2H), 4.37 (broad, 4H), 3.66- 3.46 (m, 56H), 3.29 (broad, 12H), 2.62 (broad, 2H). The molecular weight could not be determined due to strong aggregation of polymer in solution.

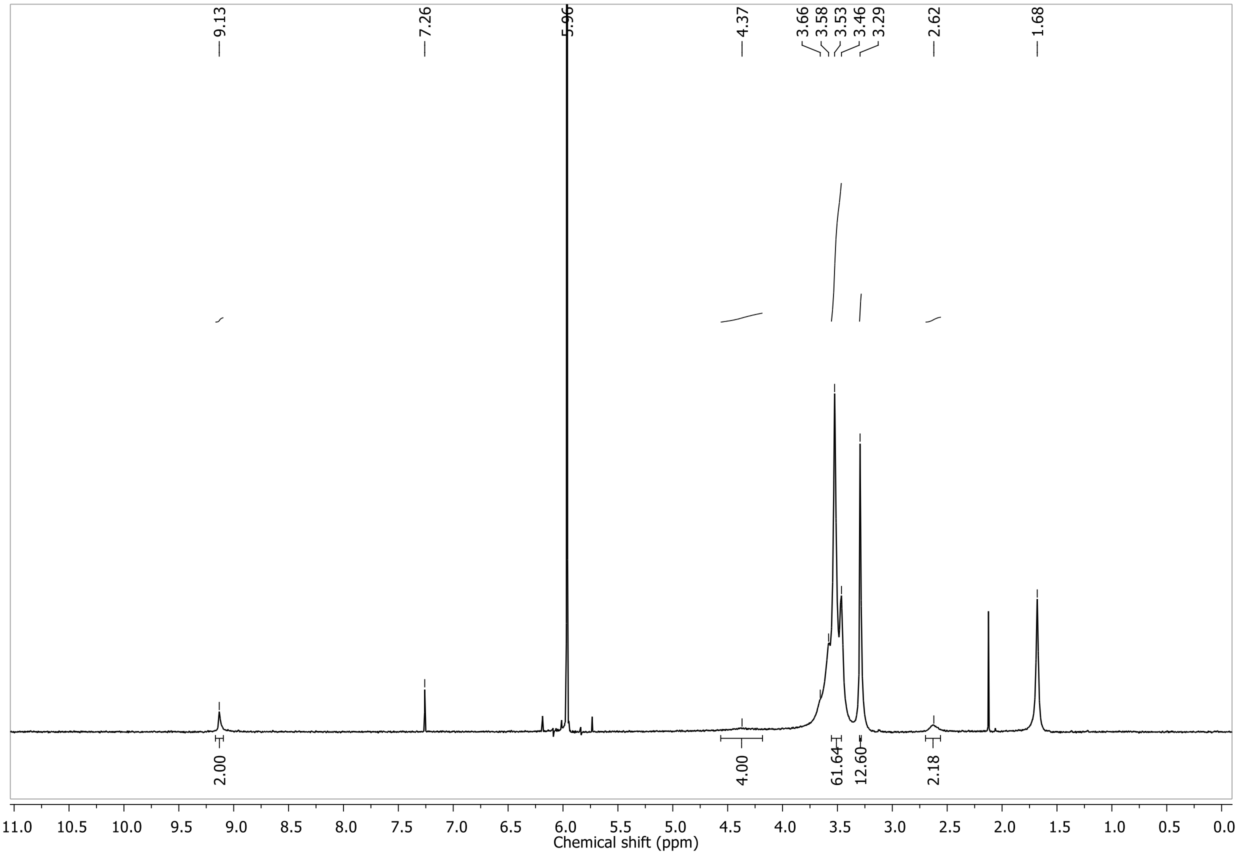

Figure S3: ^{1}H NMR spectrum of polymer P3G in TCE-*d*$_2$ at 60 °C.

Density functional theory (DFT) Calculations: The DFT calculations were carried out using Becke's three-parameter gradient-corrected functional (B3LYP) with 6-31G(d,p) basis set for the optimizations of geometric structures and calculations of energy levels.[2]

Device Fabrication:

Glass substrates were sequentially sonicated in soapy water, DI water, acetone, and isopropanol, dried using a nitrogen gun and cleaned with oxygen plasma for 10 min. The doped films were prepared by spin-coating a solution of the conjugated polymer (10 mg mL^{-1} in chloroform) mixed with different amounts of N-DMBI solution (10 mg mL^{-1} in chloroform) in a glove box with nitrogen atmosphere. The molar concentration is calculated considering the molecular weight of N-DMBI and the molecular weight of the repeating unit in each polymer. Electric conductivity was measured using a voltage-sourced two-point probe method with pre-patterned bottom contact Au electrodes (Scheme S1). An average of 18 devices were tested for each host-dopant ratio. The measurements were conducted using a probe station in an N2 glove box. The electrical conductivity (σ) was calculated according to the formula: $\sigma = (I/V) \times L/(w \times d)$. The thickness of the films was acquired through AFM.

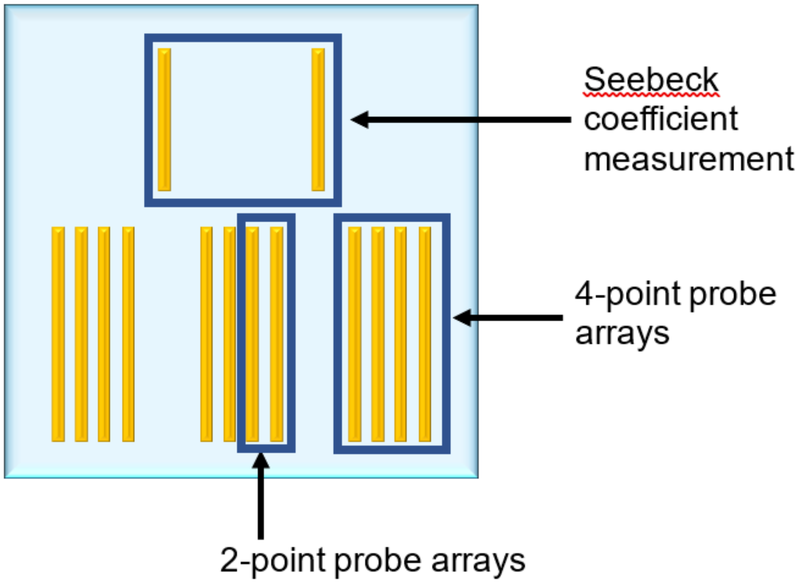

Scheme S1: Device geometry for electrical conductivity and Seebeck coefficient determination. The device geometry allows to perform both 2-point probe and 4-point probe measurements.

Characterization of the films:

Absorption spectra were collected using a Cary 5000 UV-Vis-NIR spectrometer. EPR was collected using a continuous-wave Bruker ELEXSYS E500 electron paramagnetic resonance (EPR) spectrometer operating at the X band (microwave frequency, 9.7–9.9 GHz), equipped with a super high Q resonator (ER 4122 SHQ) was used to record all EPR spectra. Thin-film samples were prepared on a flexible substrate and sealed in EPR tubes within a nitrogen-filled glovebox. The spectra were measured using the same conditions for all samples. Bruker Xenon software (Bruker BioSpin, Rheinstetten, Germany) was used to collect the data, post-processing, and spin counting. AFM images were recorded in semi-contact mode using a Next-Solve by MD-NDT with OTESPA cantilevers from Bruker (nominal tip radius 10 nm). Contact angle measurements were performed on Kruss-DSA100.

Photoelectron Spectroscopy:

Thin-film polymer samples were prepared by spin coating polymer sol. in $ChCl_3$ (2mg/mL) on a clean silicon substrate coated with a 10nm Ti adhesion layer and 100nm of gold.

UPS measurements on thin polymer films were performed in an ultrahigh vacuum chamber (base pressure of 10^{-10} mbar) equipped with a Sphera II EAC 125 7-channeltron electron analyzer calibrated with the Fermi edge of clean polycrystalline silver. The spectra were recorded at a pass energy of 10 eV using the He I line (21.22 eV). The work function of the samples was determined from the secondary electron cut-off of the UP spectra, as described elsewhere, with an uncertainty of ± 0.05 eV.[3]

LEIPES measurements were performed in isochromatic mode (base pressure 10^{-9} mbar) using an in-house build setup using a solid-state PMT detector (Hamamatsu R585) mounted outside of vacuum and equipped with a bandpass filter of 280 nm (Semrock) with a narrow wavelength window of 10 nm. The system is based on a setup previously reported by H. Yoshida in 2012.[4] LEIPES measurements were performed on the same samples after the UPS measurements, in an interconnected ultrahigh vacuum chamber without breaking the vacuum. The onset energies of frontal molecular orbitals were estimated by de-convoluting the spectra using Gaussian functions and a Tougaard background.

X-ray scattering:

The polymer films for X-ray scattering were spin-coated on polished silicon with native SiO_2. Grazing Incidence Wide Angle X-ray Scattering (GIWAXS) was performed in a Xenocs Xeuss 2.0 beamline with Cu Kα radiation λ=1.54 Ǻ. The scattered beam was collected by a Pilatus 1M detector. The total exposure time was 3 hours per sample.

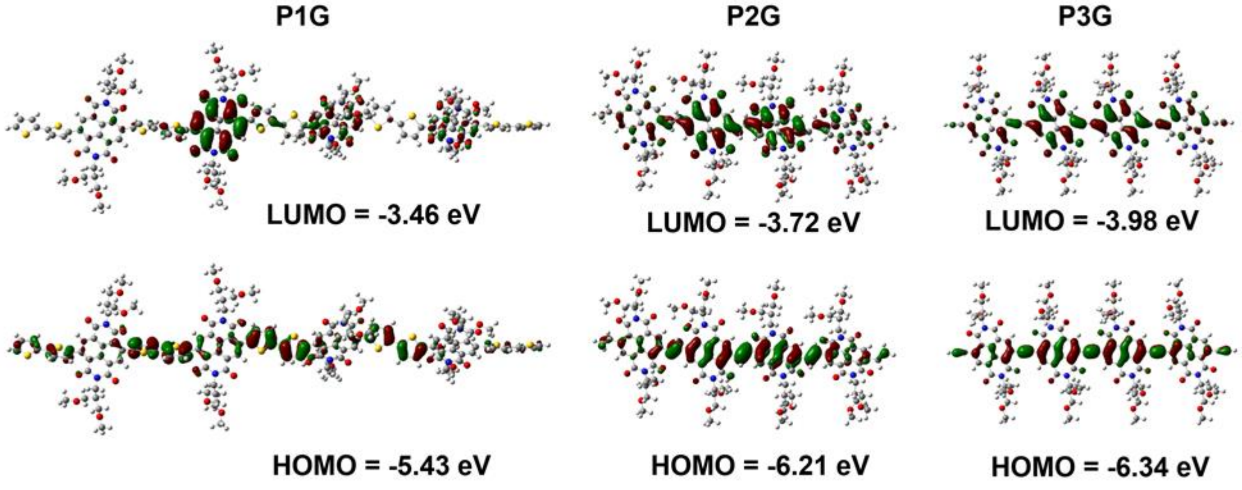

Figure S4. Energy levels of the frontier molecular orbitals of the CPs calculated using DFT.

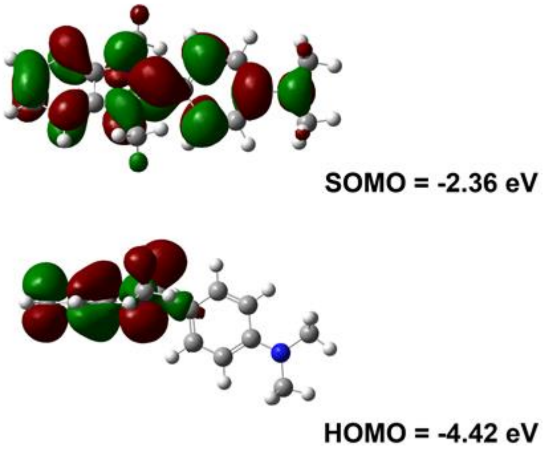

Figure S5. Energy levels of the HOMO and SOMO of N-DMBI

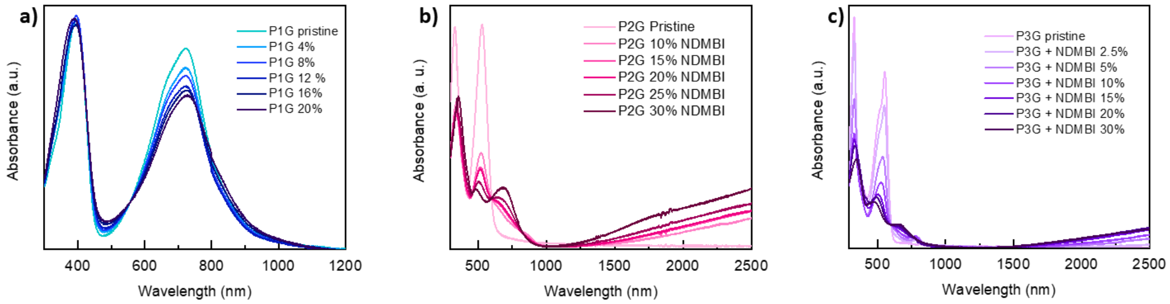

Figure S6. UV-Vis-NIR spectra of the pristine and doped thin films a) P1G, b) shows P2G and c) P3G, both showing strong polaronic and bipolaronic transitions in the NIR.

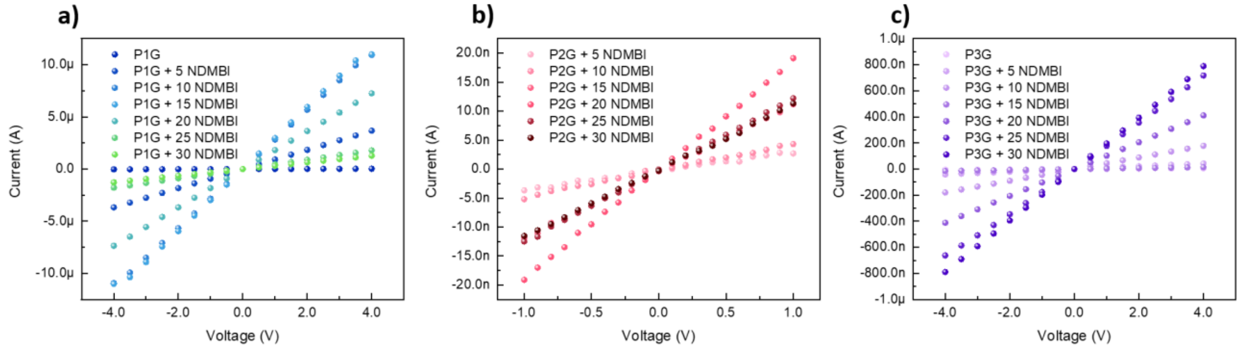

Figure S7. Representative I-V curves of the polymer films used to calculate their electrical conductivities. a) P1G, b) P2G and c)P3G.

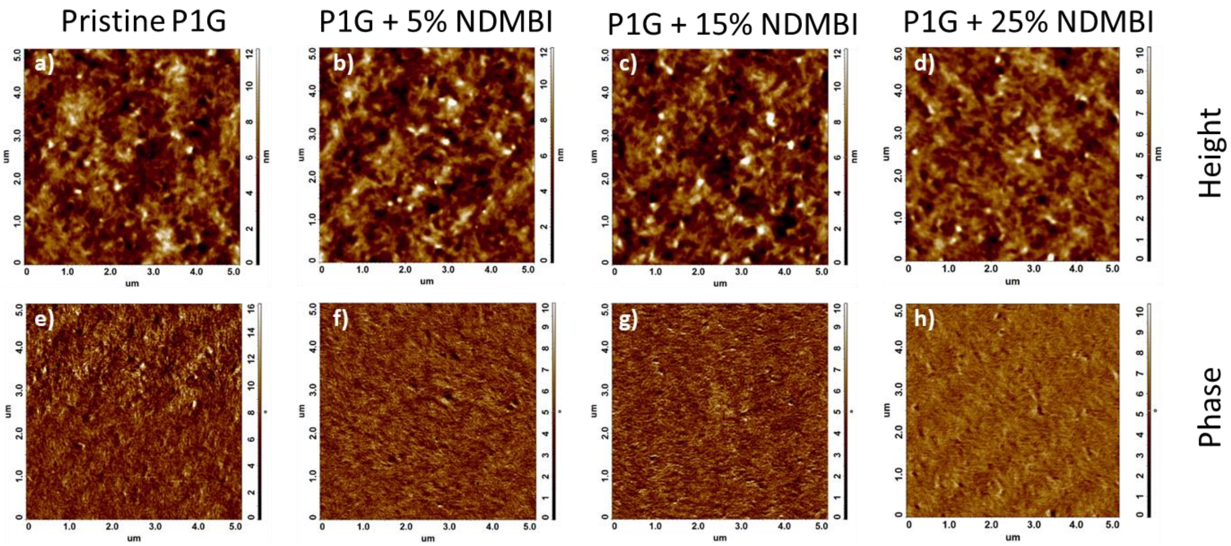

Figure S8. AFM topography and phase images for the pristine and doped P1G films.

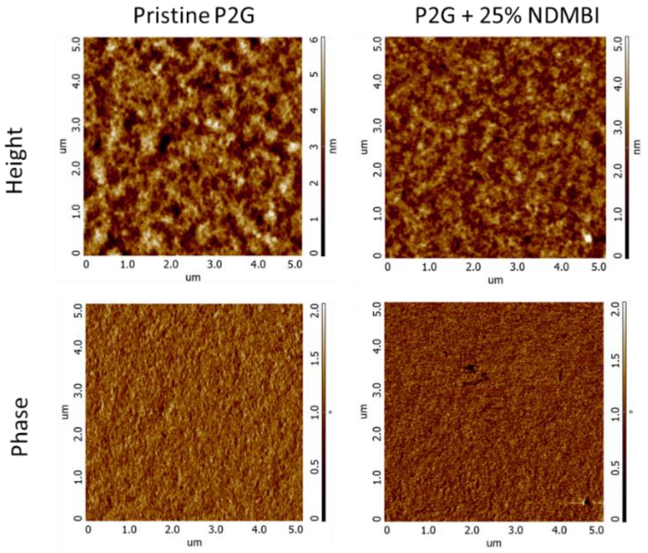

Figure S9. AFM topography and phase images for the pristine and doped P2G films.

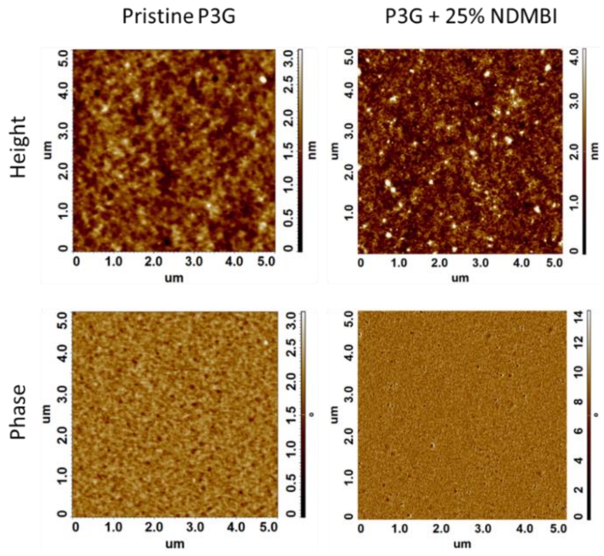

Figure S10. AFM topography and phase images for the pristine and doped P3G films.

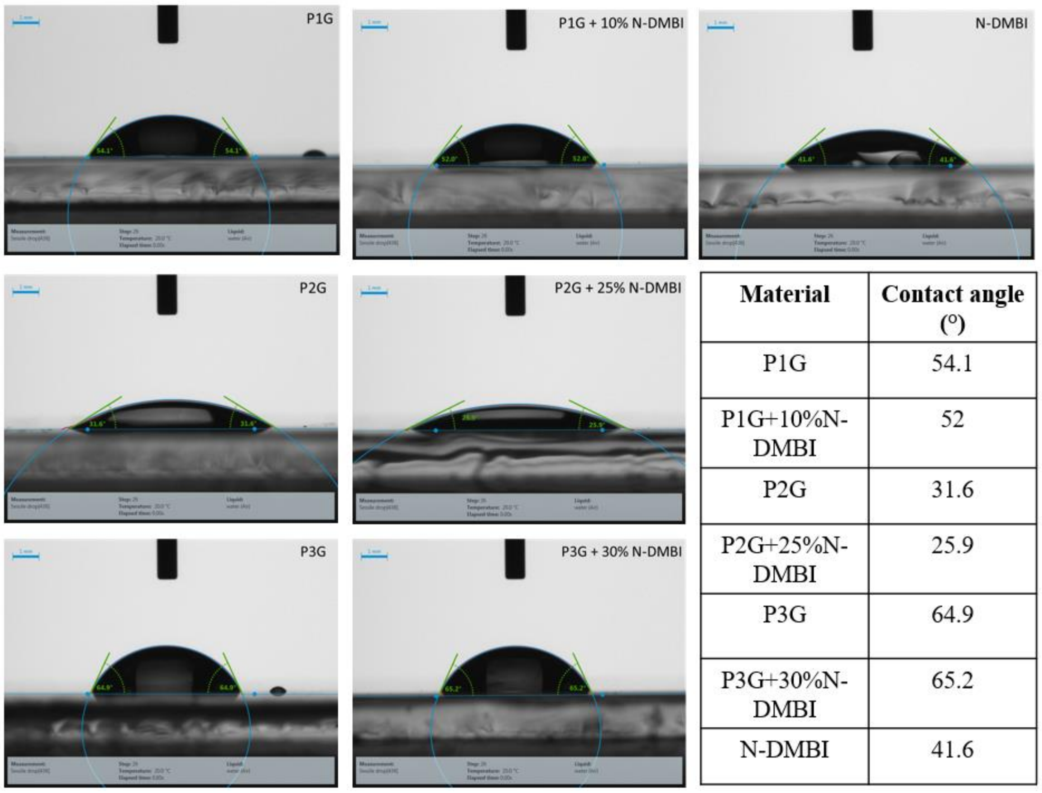

Material	Contact angle (°)
P1G	54.1
P1G+10%N-DMBI	52
P2G	31.6
P2G+25%N-DMBI	25.9
P3G	64.9
P3G+30%N-DMBI	65.2
N-DMBI	41.6

Figure S11. Contact angle measurements of undoped polymer films, N-DMBI dopant, and polymer-dopant blends at the ratio resulting in the highest σ. The droplet is water.

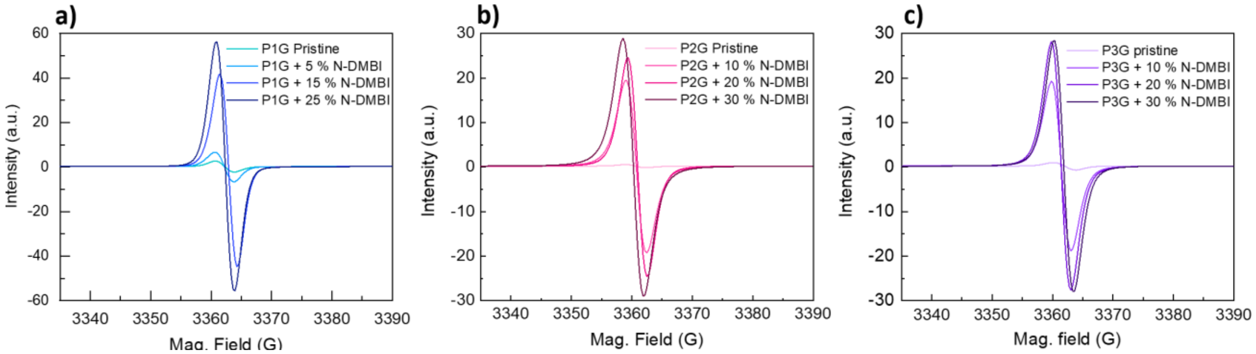

Figure S12. EPR spectra of pristine and doped polymer films for a) P1G, b) P2G, and c) P3G.

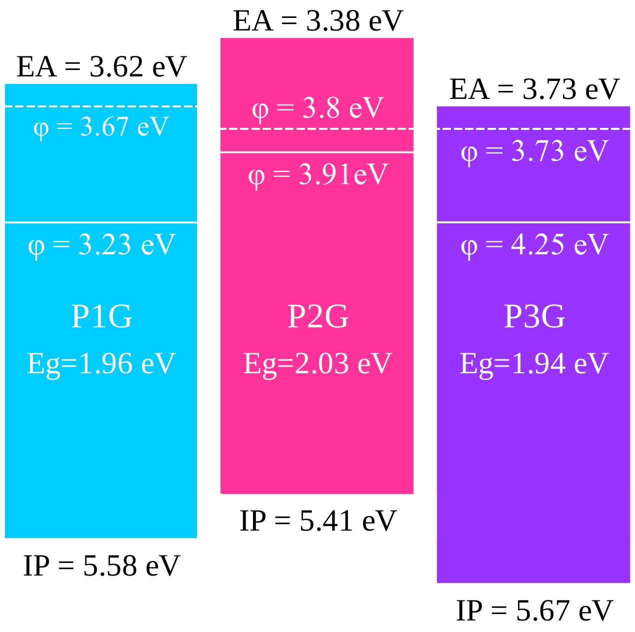

Scheme S2. Diagram of the energy levels for the three polymers as obtained from photoelectron espectroscopy. Work function before doping is depicted with a solid line, and with dashed lines for doped samples. The shift toward vacuum level demonstrates n-type doping.

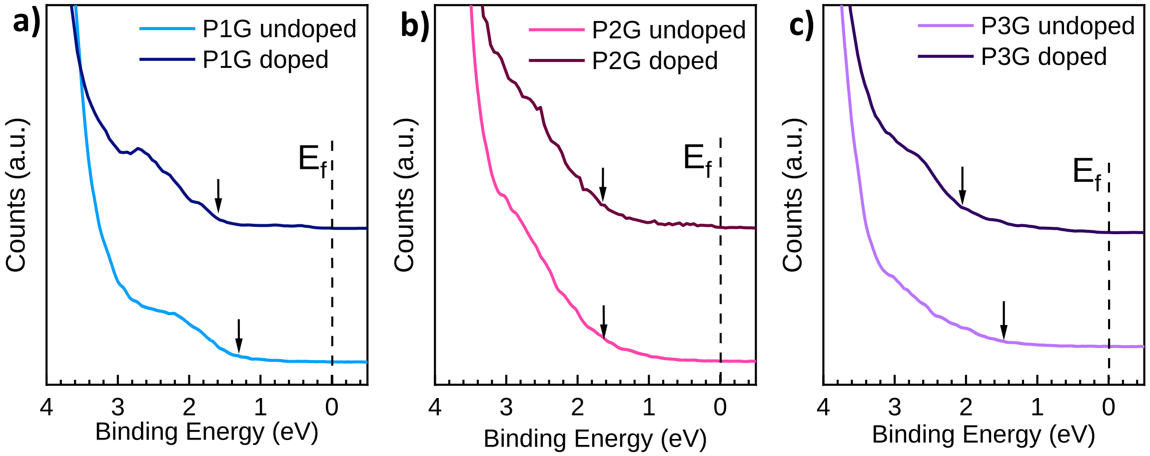

Figure S13. UPS of the pristine and doped polymer films. a) to c) show the s.e. cut-off region with the work function. d) to f) show the IE or valence region.

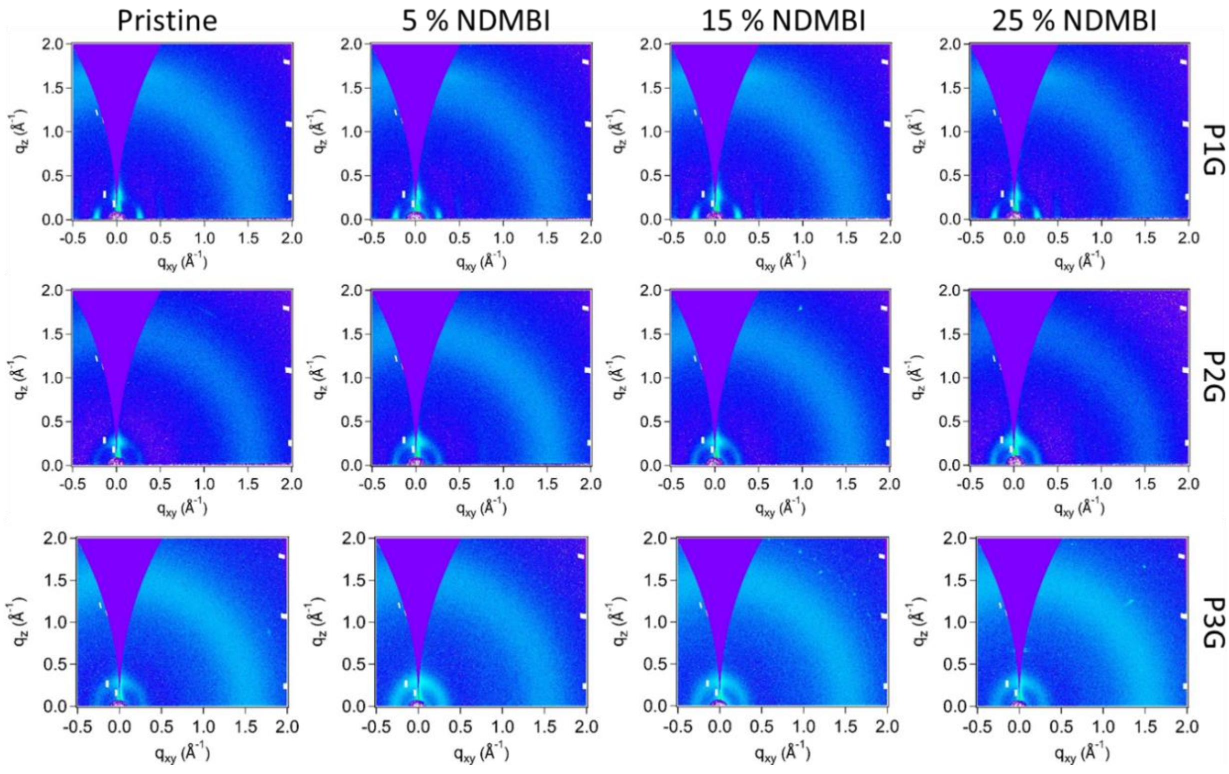

Figure S14. GIWAXS 2D contour plots for pristine and doped polymers.

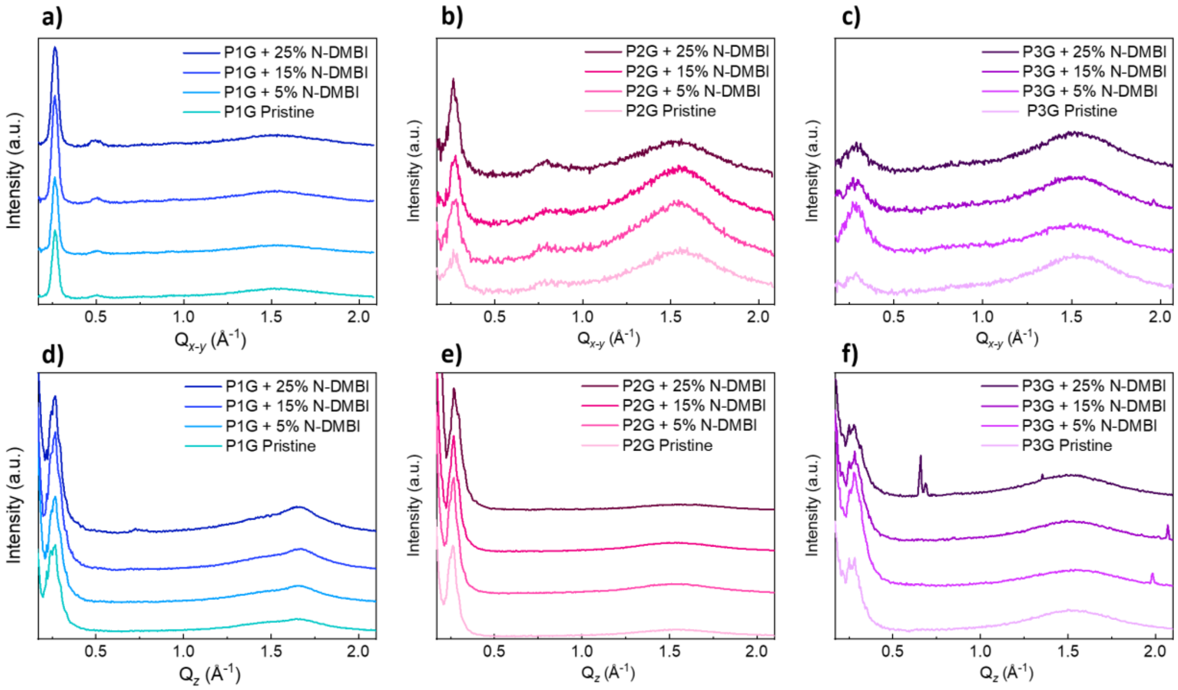

Figure S15. GIWAXS Linecuts for pristine and doped polymers.

sample	100	200	300	
P1G	0.26618	0.50544	0.71397	0.92873
P1G 5% N-DMBI	0.26601	0.50083	0.75962	0.92312
P1G 15% N-DMBI	0.26517	0.50244	0.75667	0.93935
P1G 25% N-DMBI	0.26559	0.49628	0.76059	0.93939
P2G	0.27392		0.78607	
P2G 5% N-DMBI	0.2707		0.78249	
P2G 15% N-DMBI	0.27532		0.80396	
P2G 25% N-DMBI	0.27303		0.79529	
P3G	0.28584	0.88577	1.5353	
P3G 5% N-DMBI	0.2836	0.91236	1.5051	
P3G 15% N-DMBI	0.28044	0.78906	1.5273	
P3G 25% N-DMBI	0.28915	0.88727	1.5278	

Table S1. Summary of the scattering peaks from the in-plane linecuts. All values are in A^{-1}.

Sample	100		010	FWHM (010)
P1G	0.25861		1.5975	0.5141
P1G 5% N-DMBI	0.26454		1.6093	0.5024
P1G 15% N-DMBI	0.26286		1.6127	0.50097
P1G 25% N-DMBI	0.26402	0.73881	1.6232	0.44758
P2G	0.26206			
P2G 5% N-DMBI	0.26444			
P2G 15% N-DMBI	0.26918			
P2G 25% N-DMBI	0.27864	0.81029		
P3G	0.27933			1.5232
P3G 5% N-DMBI	0.28763			1.5252
P3G 15% N-DMBI	0.28854			1.5173
P3G 25% N-DMBI	0.28254	0.65736	0.6871	1.51

Table S2. Summary of the scattering peaks from the out-of-plane linecuts. All values are in A^{-1}.

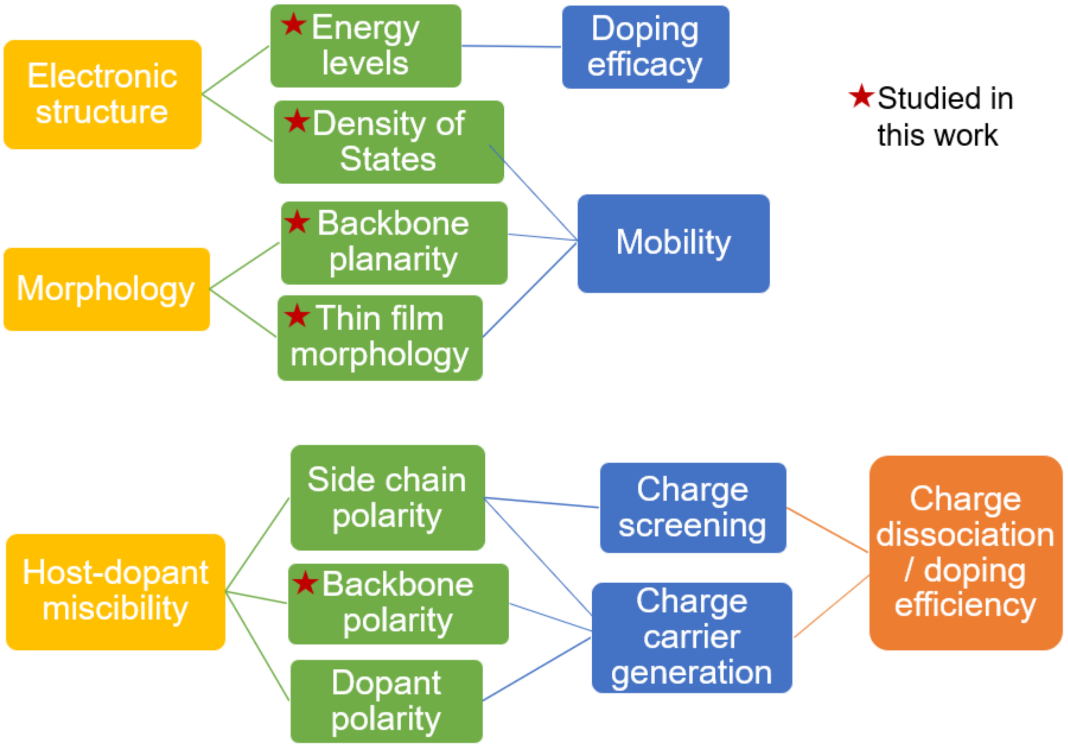

Scheme S3. Diagram correlating the factors that contribute to electrical conductivity of doped conjugated polymers.

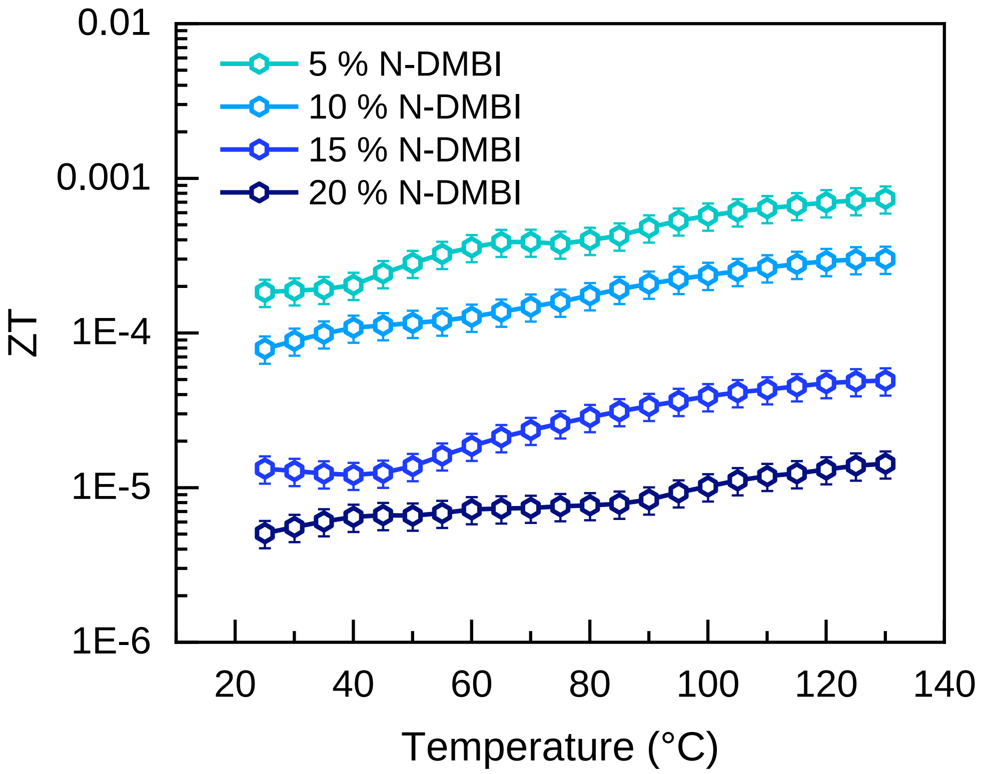

Figure S16. Thermoelectric Figure of Merit (ZT) for the doped P1G Films

References

1. A. Sharma, S. Singh, X. Song, D. Rosas Villalva, J. Troughton, D. Corzo, L. Toppare, G. Gunbas, B. C. Schroeder and D. Baran, *Chem. Mater.*, 2021, **33**, 8602-8611.
2. M. J. Frisch, G. W. Trucks, H. B. Schlegel, G. E. Scuseria, M. A. Robb, J. R. Cheeseman, G. Scalmani, V. Barone, G. A. Petersson, H. Nakatsuji, X. Li, M. Caricato, A. V. Marenich, J. Bloino, B. G. Janesko, R. Gomperts, B. Mennucci, H. P. Hratchian, J. V. Ortiz, A. F. Izmaylov, J. L. Sonnenberg, Williams, F. Ding, F. Lipparini, F. Egidi, J. Goings, B. Peng, A. Petrone, T. Henderson, D. Ranasinghe, V. G. Zakrzewski, J. Gao, N. Rega, G. Zheng, W. Liang, M. Hada, M. Ehara, K. Toyota, R. Fukuda, J. Hasegawa, M. Ishida, T. Nakajima, Y. Honda, O. Kitao, H. Nakai, T. Vreven, K. Throssell, J. A. Montgomery Jr., J. E. Peralta, F. Ogliaro, M. J. Bearpark, J. J. Heyd, E. N. Brothers, K. N. Kudin, V. N. Staroverov, T. A. Keith, R. Kobayashi, J. Normand, K. Raghavachari, A. P. Rendell, J. C. Burant, S. S. Iyengar, J. Tomasi, M. Cossi, J. M. Millam, M. Klene, C. Adamo, R. Cammi, J. W. Ochterski, R. L. Martin, K. Morokuma, O. Farkas, J. B. Foresman and D. J. Fox, *Journal*, 2016.
3. A. Sharma, G. Andersson, J. Rivnay, J. F. Alvino, G. F. Metha, M. R. Andersson, K. Zuber and M. Fabretto, *Adv. Mater. Interfaces*, 2018, **5**, 1800594.
4. H. Yoshida, *Chem. Phys. Lett.*, 2012, **539-540**, 180-185.